ACCRETION ONTO A MAGNETIC DIPOLE: RESULTS OF 2D NUMERICAL SIMULATIONS

Yu.M. Toropin[1], O.D. Toropina[2]

[1] Keldysh Institute of Applied Mathematics, Russian Academy of Sciences, Moscow, Russia; *toropin@spp.keldysh.ru*

[2] Space Research Institute, Russian Academy of Sciences, Moscow, Russia; *toropina@mx.iki.rssi.ru*

ABSTRACT. Different regimes of accretion to a star with a dipole magnetic field were investigated using 2D numerical axisymmetric resistive MHD simulations. Numerical technique was improved over our recently published results (Toropin et al., 1999, refered as T99 below).

A new model for the gravitating star with a dipole magnetic field was adopted for presented simulation set. Spherical accretion to a non–rotating star with a dipole field was modeled. Existence of the stationary accretion flow with polar columns inside the Alfvén surface was confirmed. The accretion rate to the dipole in the axially symmetric flow is always smaller than in the Bondi accretion to corresponding non–magnetized star. Relations, obtained in previous paper (T99), between the accretion rate to the non–rotating dipole $\dot{M}_{dip}$ and the magnetic momentum μ, the density of surrounding medium ρ_∞, the magnetic diffusivity η_m are qualitatively confirmed in simulations with new model of dipole. Specifically, $\dot{M}_{dip} \propto \left(\varrho_\infty / \mu^2\right)^{0.5} \cdot \eta_m^{0.38}$ and the Alfvén radius is $R_A \propto \left(\varrho_\infty / \mu^2\right)^{-0.3} \cdot \eta_m^{0.07}$.

Investigations of the cylindrical accretion (parrallel to the star's magnetic momentum) were started. If the value of the star's gravitational capture radius is close to its Alfvén radius then the magnetic field surves as an effective obstacle for the incoming flow deflecting it from the star. Simulated flow structure is discussed.

Key words: accretion; dipole; MHD; OINS

1. Introduction

A general analytic solution for spherical accretion to a non–magnetized star was obtained by Bondi (1952). His results were confirmed recently with the help of numerical three–dimensional (3D) hydrodynamic simulations by Ruffert (1994). Accretion of matter with low angular momentum to non–magnetized center was investigated by Bisnovatyi–Kogan & Pogorelov (1997).

Less attention has been given to quasi–spherical accretion to a *magnetized star*. Although in many cases accretion occurs through a disk, in other cases, where accreting matter has small angular momentum the accretion flow is quasi–spherical. Examples include some types of wind fed pulsars (see review by Nagase 1989). Also, quasi–spherical accretion may occur to an isolated star (especially, to an Old Isolated Neutron Star, OINS) if its velocity through the interstellar medium is small compared with the sound speed.

Due too intristic multidimensional nature of accretion flow to the dipole and nonlinearity of MHD equations only numerical calculations could unveil darkness from the real flow structure. Questions of interest are:

- the position & the shape of the Alfvén surface;
- the departures of the flow from spherical inflow to highly anisotropic polar column accretion inside the dipole's magnetosphere;
- dependence of the accretion rate to the dipole on the star's magnetic momentum and rotation rate, the sorrounding matter's density and the magnetic diffusivity (considered by Lovelace et al. 1995 for the case of disk accretion).

In our recent work (T99) a spherical accretion to a rotating star with an aligned dipole magnetic field was investigated by 2D MHD numerical simulations. In this paper development of that investigations with an improved dipole model is presented.

2. Model

Axisymmetric MHD simulations of spherical and cylindrical accretion to a (rotating) star with an aligned dipole magnetic field were performed under following approach. We consider the equation system for resistive MHD,

$$\frac{\partial \rho}{\partial t} + \nabla \cdot (\rho\ \mathbf{v}) = 0\ , \qquad (1)$$

$$\rho \left(\frac{\partial \mathbf{v}}{\partial t} + (\mathbf{v} \cdot \nabla) \cdot \mathbf{v} \right) = -\nabla p + \frac{(\mathbf{J} \times \mathbf{H})}{c} + \mathbf{F}^g, \qquad (2)$$

$$\frac{\partial \mathbf{H}}{\partial t} = \nabla\times(\mathbf{v}\times\mathbf{H}) + \frac{c^2}{4\pi\sigma}\nabla^2\mathbf{H}\ , \qquad (3)$$

$$\frac{\partial(\rho\varepsilon)}{\partial t} + \nabla\cdot(\rho\varepsilon\mathbf{v}) = -p\,(\nabla\cdot\mathbf{v}) + \frac{\mathbf{J}^2}{\sigma}\ . \qquad (4)$$

All variables had their usual meanings. The equation of state was considered to be that for an ideal gas, $p = (\gamma-1)\,\rho\varepsilon$, with $\gamma = 7/5$ the usual specific heat ratio. The equations incorporated Ohm's law $\mathbf{J} = \sigma(\mathbf{E} + \mathbf{v}\times\mathbf{H}/c)$, where σ was the electrical conductivity. The corresponding magnetic diffusivity $\eta_m \equiv c^2/(4\pi\sigma)$ was constant in whole calculation region.

We used an inertial cylindrical coordinate system (r, ϕ, z), its origin coincided with the star's and dipole's centers, the z–axis was parallel to the star's rotation axis and dipole magnetic momentum μ. Axisymmetry was assumed, $\partial/\partial\phi = 0$, and the z–axis was threated as a symmetry axis.

In order to guarantee that $\nabla\cdot\mathbf{H} = 0$ holds for all time in the numerical simulations, we used the vector potential $\mathbf{A}$ for the magnetic field, $\mathbf{H} = \nabla\times\mathbf{A}$, instead of magnetic field $\mathbf{H}$ itself. The magnetic field of the central gravitating object was chosen as an exact dipole one, $\mathbf{A} = \mu\times\mathbf{R}/R^3$. The corresponding magnetic field was $\mathbf{H} = [3\mathbf{R}\,(\mu\cdot\mathbf{R}) - R^2\mu]/R^5$, which was a **"pure" dipole** field.

This was the main methodological advantage over the dipole's model in (T99) where the magnetic potential was builded up as a potential of a "current" disk with a small but finite size placed in the equatorial plane. With the "point" dipole, used in describing simulations, we usually observed more narrow polar columns in comparison with previously published results with dipole, created by the distributed electric current system (T99). This could be explained by better convergence of the field lines to the axis in the star's vicinity in the case of the point dipole.

In eq. (2) the gravity force $\mathbf{F}^g(\mathbf{R}) = -GM\rho\mathbf{R}/R^3$, is due to the central star, where $\mathbf{R}$ is the radius vector, and M is the star's mass. The gravity force and the magnetic potential without softering were used because a totally absorbing object, an "accretor" was placed close around the origin. Its surface could be treated as a star's surface that absorbs all accreted matter. The size of the accretor was chosen to be small, $r_{accr} << R_{max}$. We were experimenting with "accretors" of two sorts (see Fig. 1 and compare to Fig. 1 from T99). The first one is a coarse approximation of the sphere on rectangular grid, the second one is the simplest case with square shape accretor. Test simulations showed very small differences in flow around these two accretors, in fothcoming text only simulations with the square accretor will be described.

The magnetic potential was fixed on the surface of the accretor during whole simulation. This followed from the electromagnetic conditions on the surface of the perfectly conductingh star and protected the star's magnetic field against destruction (T99). Full descriptions of set method for the boundary conditions on the star's surface could be found in T99.

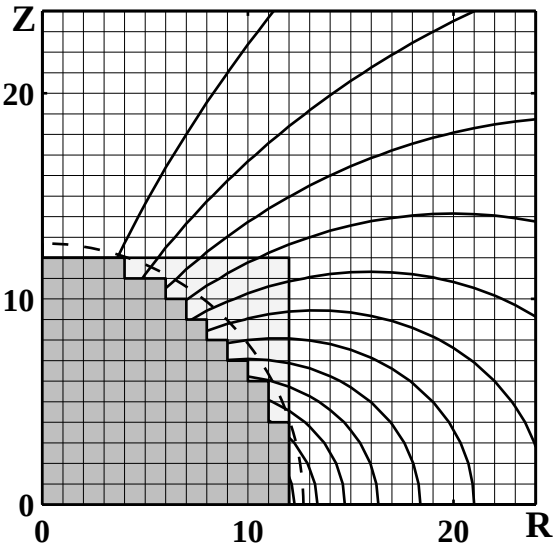

Figure 1: A scheme of the "accretor" for two cases, a coarse approximation to the circle and a square shaped "accretor" together with the dipole magnetic field lines are presented. Only 25×25 cells around the origin of the whole 257×257 calculation grid are shown.

Two dimensionless plasma parameters define the solution of the equations (1)–(4) after reduction to the dimensionless form. The first parameter is

$$\beta \equiv \frac{8\pi P_\infty}{H_0^2} \propto \dot{M}_B/\mu^2\ . \qquad (5)$$

The important quantity $\dot{M}_B/\mu^2$ is referred to as the "gravimagnetic" parameter by Davies & Pringle (1981). The second parameter is

$$\tilde{\eta}_m \equiv \frac{\eta_m}{R_A V_A} = \frac{1}{Re_m}\ . \qquad (6)$$

– dimensionless magnetic diffusivity. The third parameter connected to gravity is "hidden" by choosing Bondi radius $R_B = GM_\star/\,c_\infty^2$ as a scale unit.

3. Results

3.1. Spherical accretion onto a magnetic dipole

Symmetry about the $z = 0$ plane was assumed for spherical accretion onto a dipole and so it was possible to perform they in one quater of the (r, z) plane. Typically an equidistant orthogonal grid with 257×257 resolution was used.

Following boundary conditions were adopted. The region of the equatorial plane $(0 < r \le R_{max}, z = 0)$

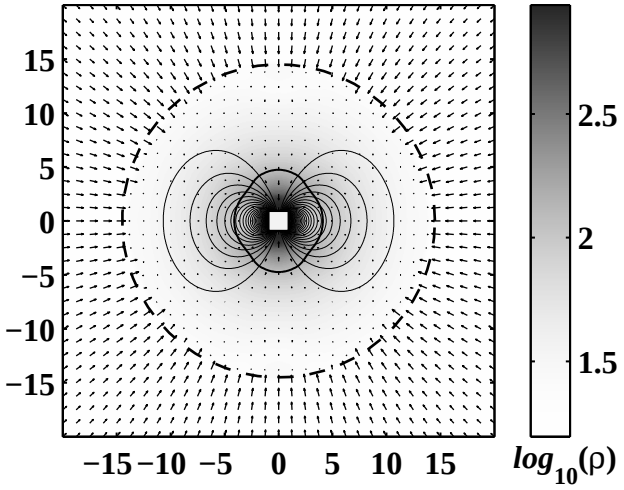

Figure 2: Simulation of the spherical accretion onto a non–rotating dipole. Position of the shock wave is marked by the dashed line and the Alfvén surface is marked by solid line, its equatorial radius is $R_A^{eq} \approx 4.1R_\star \approx \frac{1}{35}R_B$. Calculation grid is 257×257, vectors are drawn at every 32nd knot at every directions.

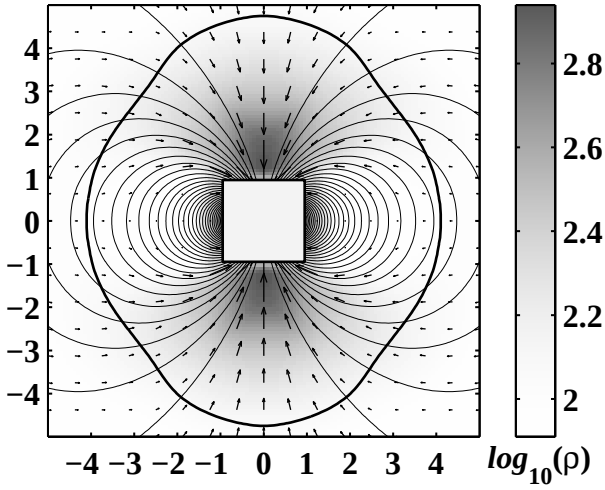

Figure 3: Vicinity of the magnetized accreting object. The Alfvén surface is marked with the solid line and inside it matter flows along the magnetic field lines. Polar columns accretion could be seen on this picture. Vectors are drawn at every 8th point along both directions, $\beta = 10^{-5}$, $\eta_m = 10^{-4}$.

was treated as a symmetry plane. The z–axis was treated as a symmetry axis. For outer boundaries we assume spherically symmetrical inflow with physical values given by the classical Bondi (1952) solution with maximum possible accretion rate

$$\dot{M}_B = 4\pi\lambda \left(\frac{GM}{c_\infty^2}\right)^2 \rho_\infty c_\infty \ , \qquad (7)$$

defined by the density ρ_∞ and the sound speed c_∞ at infinity and by the mass of the central object M. Bondi solution gave physical parameters for the inflow boundaries ($r = R_{max}$, $0 \le z \le Z_{max}$) and ($0 \le r \le R_{max}$, $z = Z_{max}$). Computational region lies inside the sonic surface $R_{max} = Z_{max} = 20R_\star = R_S/\sqrt{2}$, where the sonic radius is $R_S = (5-3\gamma)/4R_B$, and $R_B = GM/c_\infty^2$ is the Bondi radius. The accretion is supersonic, all gas dynamical variables could be fixed at the outer boundaries.

Simulations for different values of $\beta \propto \dot{M}_B/\mu^2$ and magnetic diffusivity η_m were performed. We can make following conclusions based on simulations.

Spherical accretion to a magnetic dipole is very different from that to a non–magnetized star. Instead of supersonic steady inflow, which is observed in standard Bondi accretion, a shock wave forms around the dipole just after begin of simulation. The supersonic inflow outside the shock becomes subsonic inside it. In all cases we observe that the shock wave gradually expands outwards. Figure 2 shows the main features of the flow at time when the shock has moved to the distance $R_{sh} = 14R_\star$.

We observe that for $R > R_{sh}$ the flow is unperturbed Bondi flow, used as initial and boundary conditions, whereas inside the shock for $R < R_{sh}$ it is subsonic. Initially, the subsonic accretion to dipole is spherically symmetric, but closer to the dipole it becomes strongly anisotropic. Near the dipole matter moves along the magnetic field lines and accretes to the poles in two polar columns. Figure 3 shows the inner subsonic region of the flow in greater detail. The dashed line shows the Alfvén surface, which we determine as the region where the matter energy–density $W = \rho(\varepsilon + \mathbf{v}^2/2)$ is equal to the magnetic energy–density $E_m = \mathbf{H}^2/(8\pi)$.

New method of central star setup (see section 2) allowed **to define the shape and sizes of the Alfvén surface more**. It is ellipsoidal, but in contrast with our previous simulations (see T99), it's more elongated along the poles. For simulations, presented on figures 2 and 3, the equatorial radius of the Alfvén surface is $R_A^{equ} \approx 4.1R_\star$, while its polar size along the symmetry axis z iz $R_A^z \approx 4.8R_\star$. This could be explained by the fact that electromagnetic energy density near the axis is higher in the field of the "point" dipole, used in this simulations set, in comparison to the energy of the field, created by the distributed current system, used in T99. But this correction is not too high, the Alfvén surface polar radius differs only by ≈ 30 % in two simulations, while the equatorial radius is around the same.

A significant deviation from spherically symmetric flow is observed for $R \le 2R_A$, because magnetic field starts to influence the flow before it reaches the Alfvén surface. The initial vacuum dipole magnetic field is

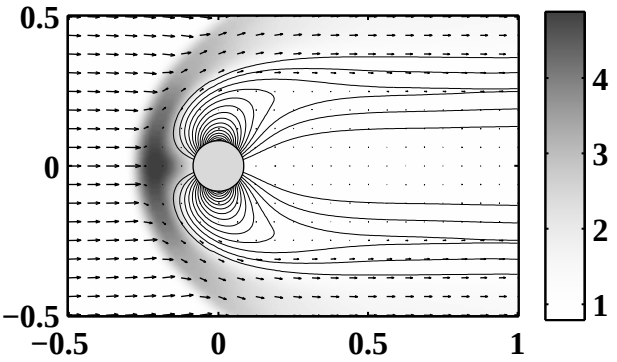

Figure 4: Cylindrical supersonic accretion to the non–rotating dipole (weak gravity case, $R_A \approx 0.25 R_B$). Density distribution in greyscale, magnetic field lines and velocity vectors at every 16th knots are shown. Mach's number is 3.

compressed inside by the accreting matter. A new stationary subsonic solution is formed around the dipole (the complete description of its pattern could be found in T99). The stationary accretion rate to the dipole $\dot{M}_{dip}$ could be measured from the simulation results.

As was pointed out first in T99, the accretion rate to the dipole is always smaller than to corresponding non–magnetized star, even if the dipole is not fast rotating. For the system, discussed here and shown on illustration, the accretion rate is $\dot{M}_{dip} \approx 0.17 \dot{M}_B$ when $R_A^{equ} \approx 4.1 R_\star$. The accretion rate to the dipole was found to be depended on the magnetic momentum of the star, the surrounding density and the magnetic diffusivity as

$$\dot{M}_{dip} \propto \left(\varrho_\infty / \mu^2\right)^{0.5} \cdot \eta_m^{0.38} \ . \qquad (8)$$

The equatorial Alfvén radius varries as

$$R_A^{equ} \propto \left(\varrho_\infty / \mu^2\right)^{-0.3} \cdot \eta_m^{0.07} \ . \qquad (9)$$

Combining equations (**??**) and (**??**) with the fact that when the Alfvén radius equals to $\sim 4 R_\star$ the dipole accretion rate $\dot{M}_{dip}$ is equal to $\sim 0.17 \dot{M}_B$, we can immediatly estimate the accretion rate for systems with stronger magnetic field. For example, if the Alfvén radius will be $R_A \approx 100 \cdot R_\star$ for isolated neutron star accreting quasi–spherically from surrounding medium the accretion rate (and accretion luminosity, in advance) will be less than 1% of the Bondi's accretion rate. So, corrections needed when studing possibility of finding old isolated neutfon stars (OINS) (see, for ex., Treves & Colpi, 1991, Blaes & Madau, 1993) and they will lead to decreasing of the number of principally observable OINS by $2 \ldots 3$ order of magnitude.

3.2. Cylindrical accretion to the dipole

Simulations of the cylindrical accretion in 2D axially symmetric formulation are limited only by the flows where velocity of the matter according to the star (or vice verse) is parrallel (or antiparrallel) to the magnetic momentum of the aligned dipole.

Simulations were performed in a rectangular box ($Z_{min} \le z \le Z_{max}, 0 \le r \le R_{max}$) of the ($r$–$z$) plane, covered with a 129×385 equidistant grid with equal steps along r and z axes. The gravitating accretor with dipole magnetic field frozen ib its surface was anchored at the origin of cylindrical coordinate system. Next set of boundary conditions was used. Supersonic inflow with Mach number $M = 3$ with temporary constant accretion rate was set up on the upstream (left on the fig. 4) boundary ($z = Z_{max}, 0 \le r \le R_{max}$). On the outer cylindrical boundary ($Z_{min} \le z \le Z_{max}, r = R_{max}$ and on the downstream boundary ($z = Z_{min}, 0 \le r \le R_{max}$) so called "free boundary conditions" (i.e., $\partial / \partial \mathbf{n} = 0$) were implied.

First, the case of relatively strong magnetic field and weak gravity was investigated (see results at fig. 4). This simulation is characterezed by foolowing relations: $R_\star = R_{accr} \approx 0.1 \cdot R_B$, $R_A \approx 0.25 \cdot R_B$, where $R_B = GM/c_\infty^2$ is the Bondi radius. In corresponding hydrodynamical simulation of cylindrical accretion to non–magnetized star (see Ruffert 1994, 1995) the head conical bow shock is attached to the accretor surface. In the dipole case the strong magnetic field serves as an obstacle, a shield for accreting matter, deflecting it from the star and preventing accretion.

What will be the accretion flow pattern if the Alfvén radius will be much smaller in comparison to the Bondi radius? For typical space condition it is estimated to be $R_A \sim 0.01 \cdot R_B$ or even less. One can proposes that there will be a conical bow shock in accretion flow far from the dipole but in the immediate vicinity of the Alfvén surface and inside it the flow will be quasi–spherical.

For investigating of such interesting system we plan to incorporate so called "nested grids" method to our code. It allows to increase resolution around the dipole but at the same time allows to use coarse grids far from it. This will allow us to model system which will be cloaser to reality, with $R_A \sim 10^2 \ldots 10^3 R_\star$ and $R_A \sim 0.01 \cdot R_B$ at the same time.

Acknowledgements. The authors are thankfull to their co–authors, Dr. Romanova, Dr. Savelyev, Dr. Chechetkin and Prof. Lovelace for long fruitfull, stimulated and productive work.

References

Bisnovatyi–Kogan G.S., Pogorelov N.V. 1997, *Astron. and Astrophys. Transactions*, **12**, 263

Blaes O., Madau P.: 1993, *ApJ*, **403**, 690
Bondi H.: 1952, *MNRAS*, **112**, 195
Davies R.E., Pringle J.E.: 1981, *MNRAS*, **196**, 209
Lovelace R.V.E., Romanova M.M., Bisnovatyi-Kogan G.S.: 1995, *MNRAS*, **275**, 244
Nagase F.: 1989, *PASJ*, **41**, 1
Ruffert M.: 1994, *ApJ*, **427**, 342
Ruffert M.: 1995, *As.Ap.Suppl.*, **113**, 133
Ruffert M.: 1996, *As.Ap.*, **311**, 817
Toropin Yu.M., Toropina O.D., Savelyev V.V., Romanova M.M., Chechetkin V.M., Lovelace R.V.E.: 1999 *ApJ*, **517**, 906 (**T99**)
Treves A., Colpi M.: 1991, *As.Ap.*, **241**, 107.